Front. Optoelectron. 2019, 12(1): 52–68
https://doi.org/10.1007/s12200-019-0910-9

REVIEW ARTICLE

A review of multiple optical vortices generation: methods and applications

Long ZHU, Jian WANG (✉)

Wuhan National Laboratory for Optoelectronics, School of Optical and Electronic Information, Huazhong University of Science and Technology, Wuhan 430074, China

Abstract Optical vortices carrying orbital angular momentum (OAM) have attracted increasing interest in recent years. Optical vortices have seen a variety of emerging applications in optical manipulation, optical trapping, optical tweezers, optical vortex knots, imaging, microscopy, sensing, metrology, quantum information processing, and optical communications. In various optical vortices enabled applications, the generation of multiple optical vortices is of great importance. In this review article, we focus on the methods of multiple optical vortices generation and its applications. We review the methods for generating multiple optical vortices in three cases, i.e., 1-to-*N* collinear OAM modes, 1-to-*N* OAM mode array and *N*-to-*N* collinear OAM modes. Diverse applications of multiple OAM modes in optical communications and non-communication areas are presented. Future trends, perspectives and opportunities are also discussed.

Keywords optical communications, optical vortices, orbital angular momentum (OAM), mode-division multiplexing (MDM), mode multicasting

1 Introduction

Optical vortices, also known as orbital angular momentum (OAM) beams, have been studied for decades. It was shown by Allen in 1992 that optical vortices comprising an azimuthal phase term $\exp(il\varphi)$, possess an OAM of $l\hbar$ per photon, where l is referred to topological charge and φ is azimuthal angle [1–3]. In recent years, optical vortices have seen wide applications in different areas, such as optical manipulation, optical trapping, optical tweezers, optical vortex knots, imaging, microscopy, sensing, metrology and quantum information processing [4–9]. Moreover, due to the intrinsic spatial orthogonality of OAM modes with different topological charge numbers, one promising prospect offered by optical vortices is in optical communications [10]. Accordingly, a series of research works on OAM modes multiplexing in optical communications have been reported recently in both free space and optical fibers [11–25].

In various optical vortices enabled applications, the generation of multiple optical vortices is always highly desired, such as optical communications, optical sensing and optical measurement [26–33]. By employing multiple optical vortices in optical communications, one can greatly increase the transmission capacity and spectral efficiency. However, in the conventional experiments, one element (e.g., spiral phase plate or spatial light modulator) can only provide one OAM mode [11], which is not scalable. The cost and complexity of the system will rapidly grow with the number of the optical vortices and resultant required multiple optical elements. Thus, it is highly desirable to develop methods for generating a large number of optical vortices with less optical elements. Moreover, simultaneous generation of multiple OAM modes using a single element from a single input Gaussian beam is also an important basic function in an OAM multicasting system.

In this review article, we focus on the methods of multiple optical vortices generation and its applications. The remainder of this article is organized as follows. Section 2 presents the methods of multiple optical vortices generation. Section 3 focuses on the application of multiple optical vortices. Finally, we give some brief discussions and perspectives of multiple optical vortices.

2 Methods of multiple optical vortices generation

Generally, there are three cases for the generation of multiple optical vortices in different applications, which

Received February 20, 2018; accepted February 28, 2019

E-mail: jwang@hust.edu.cn

are summarized in Fig. 1. The first one is 1-to-N collinear OAM modes generation. By specially designing an optical element, one can get multiple collinear OAM modes from a single input Gaussian mode, as shown in Fig. 1(a), which is usually employed in OAM mode multicasting scheme. The second one is 1-to-N OAM modes array. By inputting a Gaussian mode, one can get multiple OAM modes with preset different locations, which is illustrated in Fig. 1(b). The last one is N-to-N collinear OAM modes, which is used in OAM mode multiplexing scheme. Multiple Gaussian modes from different locations are incident on an optical element for generating multiple OAM modes, which is shown in Fig. 1(c). In this section, we will introduce multiple optical vortices generation methods for these three cases in detail.

2.1 1-to-N collinear OAM modes

By designing sliced phase patterns, Yan et al. demonstrated multiple collinear OAM modes generation with a spatial light modulator (SLM) [34]. Moreover, they also experimentally demonstrated data-carrying multicasting five and seven OAM channels from a single-input OAM channel. The approach is illustrated in Fig. 2. It has been shown that an angular amplitude aperture of central angle θ with M-fold rotational symmetry can distribute energy from the input OAM beam of charge l to multiple OAM beams having equally spaced OAM charge number of $\{\ldots, -kM + l, \ldots, -M + l, l, M + l, \ldots, kM + l, \ldots\}$ (k is an integer). Note that in the first row of Fig. 2, the aperture's transmission part has a constant phase value β_0, which results in a sinc^2-like OAM charge spectrum, centered at input OAM charge l. In the second row of Fig. 2, the aperture's transmission part is complementary to that of the first aperture, and it produces a sinc^2-like OAM charge spectrum centered at $l - 6$. In the last row, the sliced phase pattern can be viewed as the superposition of the transmission parts of the above two amplitude-phase apertures. As a result, the output spectrum of the sliced phase pattern is a coherent addition of those two previous output spectra. The parameter β_0 is optimized such that most of the multicasting OAM channels have equalized power except for the two channels at the wings of the spectrum. By using this approach, 7 equally spaced OAM modes are successfully generated. The experimental results are shown in Fig. 3. By using a pattern of more slices, seven OAM channels (l = 6, 9, 12, 15, 18, 21, 24) are generated in the experiment. The phase pattern consists of three sliced regions, where there are two parameters, β_1 and β_2, to be optimized to equalize the power of the multicasting channels. The intensity patterns of before multicasting OAM mode and after multicasting OAM modes are shown in Fig. 3(a). Figure 3(b) illustrates the power distribution after multicasting.

By using the above method, one can only generate equally spaced OAM modes. However, in many applications, it is also important to generate randomly spaced OAM modes. For the simultaneous generation of n OAM modes $\{l_1, l_2, \ldots, l_n\}$, the mathematical description of the desired transmission function can be expressed as

$$f(\varphi) = \sum_{m=1}^{n} A_{l_m} \exp(\mathrm{i} l_m \varphi), \tag{1}$$

where the complex number $\{A_{l_m}\}$ comprises the weight coefficients. Normally $f(\varphi)$ is a complex form, including both amplitude and phase. To make it simplified, our work focuses on how to reduce the complex form to a phase-only function with tolerable loss in efficiency. The phase-only approximate function can be defined as $g(\varphi) = \exp[\mathrm{i}\phi(\varphi)]$ with the phase function

$$\phi(\varphi) = \mathrm{Re}\left\{ -\mathrm{i}\ln\left[\sum_{m=1}^{n} B_{l_m} \exp(\mathrm{i} l_m \varphi)\right]\right\}. \tag{2}$$

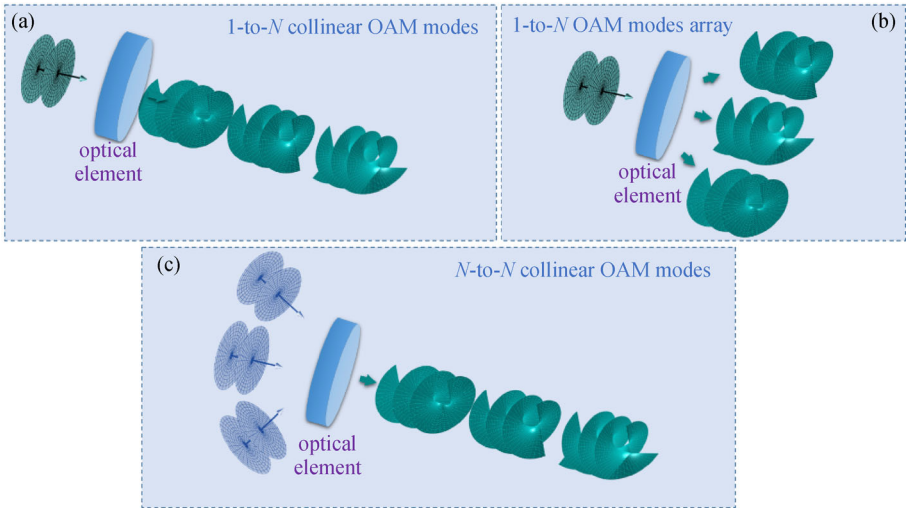

Fig. 1 Schematic illustration of multiple optical vortices generation. (a) 1-to-N collinear OAM modes; (b) 1-to-N OAM modes array; (c) N-to-N collinear OAM modes

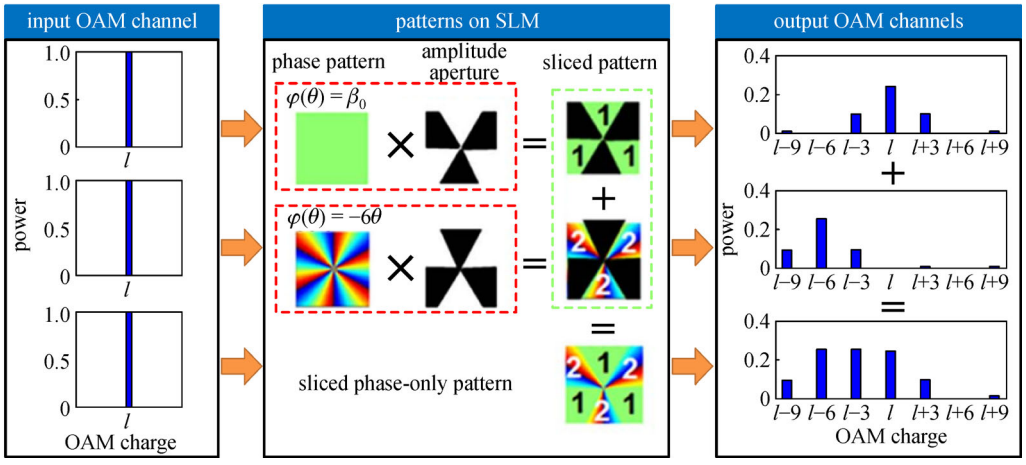

Fig. 2 Multiple OAM modes generation using an all-phase pattern with a combination of two amplitudes and a sliced phase pattern. Left: input OAM state spectrum; middle: amplitude and phase patterns for multicasting; right: generated OAM spectrum [34]

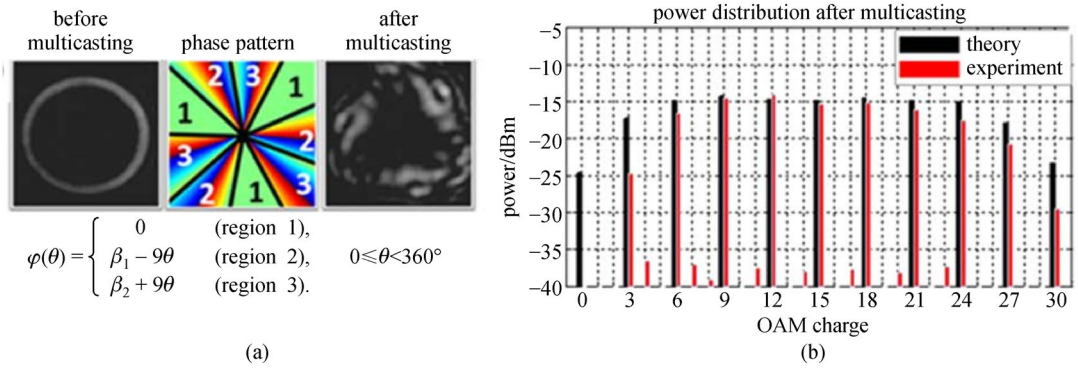

Fig. 3 Experimental results of the generated 7 equally spaced OAM modes. (a) Left: the intensity of the input OAM beam; middle: the phase pattern for multicasting; right: the intensity of the beam after multicasting; (b) theoretical and experimental results of the OAM charge spectrum after multicasting [34]

In Eq. (2), Re{ } means "real part of," and B_{l_m} is a decisive factor for $\phi(\varphi)$. Discarding the imaginary part of the right-hand side of Eq. (2) is equivalent to setting amplitude to unity, which ensures $g(\varphi)$ is a phase-only function. Expand $g(\varphi)$ in Fourier series:

$$g(\varphi)=\sum_{m=-\infty}^{\infty}C_m\exp(\mathrm{i}m\varphi), \tag{3}$$

where the decomposition coefficient is $C_m=\frac{1}{2\pi}\int_0^{2\pi}g(\varphi)\times\exp(-\mathrm{i}m\varphi)\mathrm{d}\varphi$. To achieve high efficiency, the phase-only function $g(\varphi)$ and the original function $f(\varphi)$ should be with little difference. To evaluate the difference, we introduce a parameter of relative root-mean-square error (R-RMSE):

$$\mathrm{R-RMSE}=\sqrt{\frac{\sum_{m=1}^{n}(|C_{l_m}|^2-|A_{l_m}|^2)^2}{n\sum_{m=1}^{n}|C_{l_m}|^2}}. \tag{4}$$

The smaller of the R-RMSE, the better performance of the phase-only element we can achieve.

Since the weight coefficients $\{A_{l_m}\}$ is settled at first, the parameter R-RMSE is determined by $\{C_{l_m}\}$ or $\{B_{l_m}\}$. Then it becomes a simple minimization problem. We need to find the suitable $\{B_{l_m}\}$ for minimizing R-RMSE. To solve the problem, Lin et al. proposed an iterative algorithm, which is a spontaneous optimization algorithm [35]. It is a highly effective method for generating multiple OAM modes with a single phase-only element. However, when we use this method to generate more than 10 OAM modes, the performance of the algorithm gets worse, mainly because the initial set of parameters $\{B_{l_m}^0\}$ are set equal to $\{A_{l_m}\}$. The unsuitable choice of $\{B_{l_m}^0\}$ will lead to immature convergence of the iterative algorithm.

Based on the iterative algorithm, our group proposes a pattern search assisted iterative (PSI) algorithm to simultaneously generate multiple OAM modes using a

single phase-only element [36]. The PSI algorithm shows a favorable operation performance for generating 100 randomly spaced OAM modes with high diffraction efficiency ($>93\%$), low R-RMSE and low standard deviation. Figure 4 shows the simulation results of the generated randomly spaced 100 OAM modes by PSI algorithm.

Moreover, we study the convergence of the PSI algorithm. The iterative process in the PSI algorithm is convergent. Figure 5 shows the convergence curves of R-RMSE. Figure 5(a) shows the R-RMSE convergence curve for generating 20 randomly spaced equal-power OAM modes. One can easily see from the curve that the R-RMSE is convergent after 65 iterations. The R-RMSE convergence curve for generating 50 randomly spaced equal-power OAM modes is depicted in Fig. 5(b). One can also clearly see that the R-RMSE is convergent after 91 iterations.

To evaluate the algorithm under a more realistic scenario, we study the performance of the phase patterns loaded onto the practical SLM. Here, we take commercially available Holoeye PLUTO phase only SLM as an example. The resolution of the SLM is 1920 ×1080 pixels with 256 gray levels covering $0-2\pi$ phase modulation. By using the PSI algorithm, we get realistic SLM phase patterns for generating 20 randomly spaced equal-power OAM modes. The phase pattern loaded onto SLM has 1080 ×1080 pixels with 256 gray levels, which is shown in Fig. 6(a). We then compare the performance of the realistic SLM phase pattern for generating OAM modes. The simulation results of the OAM spectra are depicted in Fig. 6(b). The OAM spectra of the original phase patterns (i.e., no consideration of realistic SLM) using PSI algorithm is also shown for reference. Figure 6(b) shows the OAM spectra of the original phase pattern (blue one) and realistic SLM phase pattern (red one) using the PSI

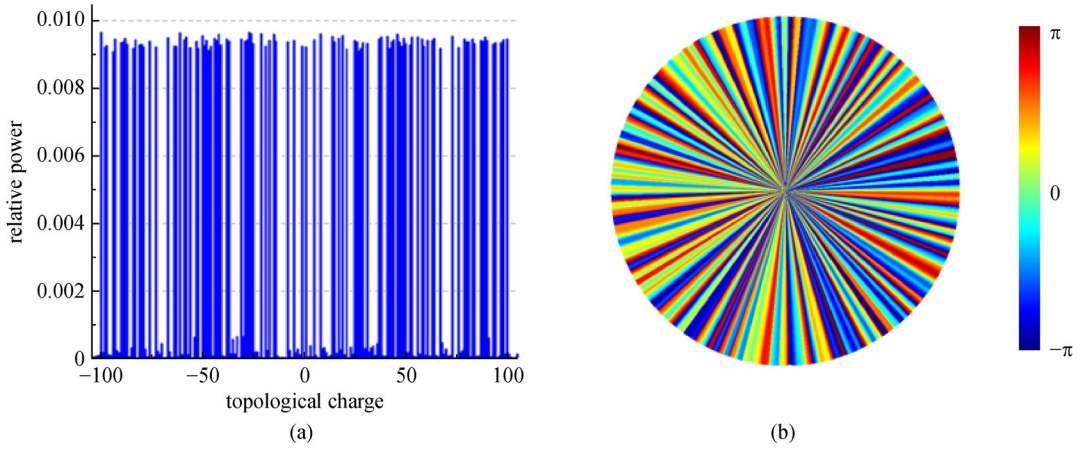

Fig. 4 Simulation results of 100 randomly spaced OAM modes with topological charge {± 1,± 5,± 8,± 14,± 15,± 17,± 19,± 21,± 25, ± 26,± 27,± 28,± 29,± 31,± 37,± 38,± 41,± 42,± 43,± 44,± 46,± 47,± 48,± 49,± 50,± 52,± 53,± 56,± 58,± 59,± 61,± 63,± 64,± 67,± 73, ± 76,± 79,± 80,± 81,± 83,± 84,± 87,± 88,± 89,± 90,± 93,± 94,± 97,± 98,± 100}. (a) 100 OAM modes spectrum by PSI algorithm; (b) phase pattern for generating 100 OAM modes by PSI algorithm [36]

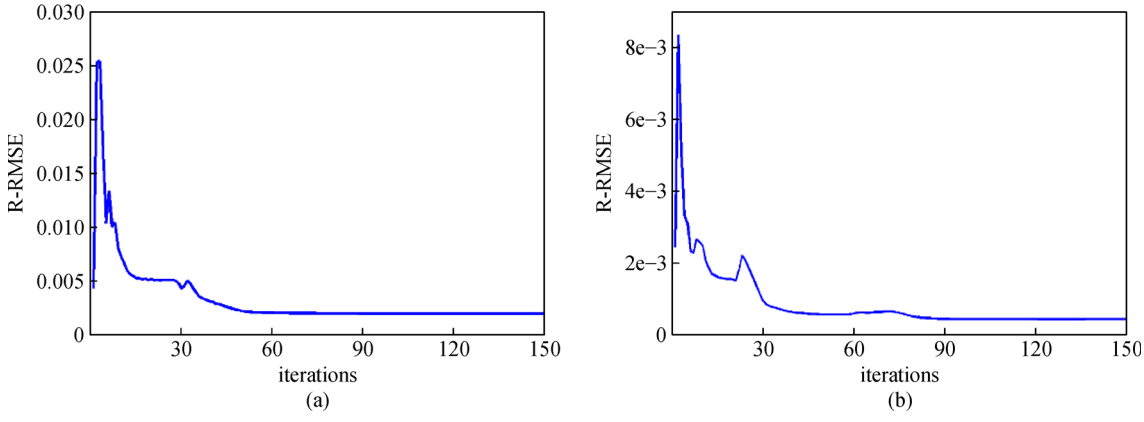

Fig. 5 R-RMSE convergence curves of PSI algorithm. (a) Convergence curve for generating 20 randomly spaced equal-power OAM modes; (b) convergence curve for generating 50 randomly spaced equal-power OAM modes [36]

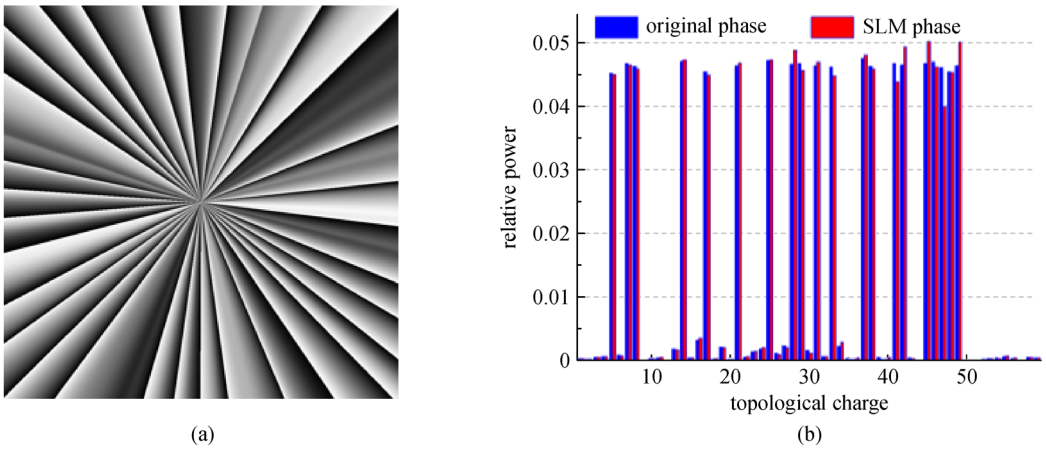

Fig. 6 (a) Phase patterns loaded onto practical SLM for generating 20 randomly spaced OAM modes with topological charge {5, 7, 8, 14, 17, 21, 25, 28, 29, 31, 33, 37, 38, 41, 42, 45, 46, 47, 48, 49} by PSI algorithm, respectively; (b) OAM spectra of the original phase pattern (blue) and realistic SLM phase pattern (red) by PSI algorithm, respectively [36]

algorithm. By comparing the simulation results shown in Fig. 6(b), one can see that the performance of realistic SLM phase pattern is slightly degraded compared with the original phase pattern.

In addition, we can also manipulate the relative power distribution of the generated OAM modes simply by setting the initial weight coefficients in the PSI algorithm. The simulation results of power manipulation of OAM modes are shown in Fig. 7.

Moreover, one can use SLMs to fully control the amplitude and phase of the input light beam, which could also be employed for the generation of multiple optical vortices. In 2014, our group proposes a simple method to arbitrarily manipulate the amplitude and phase of the incoming light beam with two phase-only SLMs without using any phase iterative algorithm [37]. The concept and principle are illustrated in Fig. 8(a). We set the polarization direction of the input light A_0 45° with respect to the x direction. The working direction of polarization-dependent SLM1 is x direction with a phase distribution $\varphi_1(x,y)$. After the SLM1, the light is half modulated, with the x direction distribution $\frac{\sqrt{2}}{2}A_0\exp(\mathrm{i}\varphi_1(x,y))$ and y direction distribution $\frac{\sqrt{2}}{2}A_0$. And then, the light beam passes through a polarizer with the polarization direction 45° deviation from the x direction. Thus, the electrical field of light beam becomes

$$E(x,y) = \frac{\sqrt{2}}{2}A_0\left(\exp(\mathrm{i}\varphi_1(x,y)) \times \frac{\sqrt{2}}{2} + \frac{\sqrt{2}}{2}A_0 \times \frac{\sqrt{2}}{2}\right)$$

$$= \frac{1}{2}A_0(\exp(\mathrm{i}\varphi_1(x,y)) + 1). \quad (5)$$

After the polarizer, the light comes through the SLM2 with a phase distribution $\varphi_2(x,y)$. The working direction of polarization-dependent SLM2 keeps the same as the light polarization after the polarizer, which is actually enabled by adjusting the light polarization after the polarizer via a half-wave plate placed between the polarizer and SLM2. So the electrical field of light after

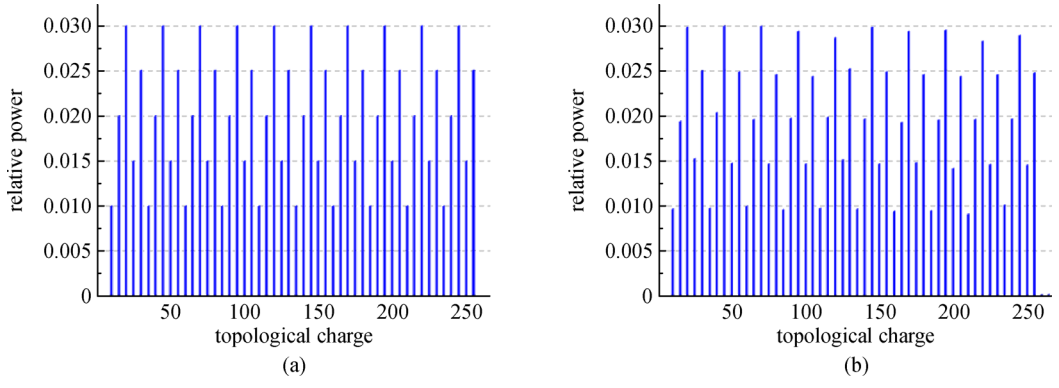

Fig. 7 Simulation results of weight manipulation of 50 OAM modes with topological charge {10, 15, 20,…, 255}. (a) Target spectrum; (b) spectrum by PSI algorithm [36]

the SLM2 becomes

$$E(x,y) = \frac{1}{2}A_0(\exp(i\varphi_1(x,y)) + 1)\exp(i\varphi_2(x,y)) = A_0\cos\left(\frac{\varphi_1(x,y)}{2}\right)\exp\left(i\frac{\varphi_1(x,y) + 2\varphi_2(x,y)}{2}\right). \quad (6)$$

From Eq. (6), one can easily find that the amplitude distribution is determined by $\varphi_1(x,y)$, and the phase distribution is determined by $\frac{1}{2}\varphi_1(x,y) + \varphi_2(x,y)$. Hence, by changing the phase distribution patterns written onto the SLM1 and SLM2, we can manipulate the amplitude and phase independently at the same time. By using this method, we show the successful generation of multiple collinear OAM modes. The theoretical and experimental results are shown in Fig. 8(b). In addition, we can arbitrarily generate different types of light beams as desired, such as Laguerre-Gaussian (LG) beams and Bessel beams. Figure 9 shows the intensity distributions of the generated LG beams and Bessel beams. The obtained results shown in Fig. 9 indicate the feasibility of arbitrary manipulation of amplitude and phase using the proposed approaches.

2.2 1-to-*N* OAM mode array

OAM mode array has found its applications in many areas, such as optical manipulation, three-dimensional scanning interferometry, and quantum processing. In 2010, Moreno et al. employed Dammann vortex grating for OAM mode array generation [38]. By combining Dammann grating with vortex phase distribution, one can get 1D Dammann vortex grating, as shown in Fig. 10(a). 2D Dammann gratings is formed by multiplying the 1D Dammann vortex grating by a 90° rotated version, which is shown in Fig. 10(c). By using Dammann vortex grating, 7 ×7 OAM mode array is successfully generated.

By employing the above method, the same group fabricates 2D Dammann grating for generating 25 OAM modes using UV lithography technique [39]. The microscopic images of the fabricated grating are shown in Figs. 11(a) and 11(b). The intensity distributions of generated OAM modes by the 2D Dammann grating are shown in Figs. 11(c) – 11(f).

Besides, our group presents a simple and compact on-chip OAM mode array emitter on silicon photonics platforms [40]. The principle relies on three-plane-wave interference. We design, fabricate and demonstrate an on-chip OAM mode array emitter consisting of three parallel

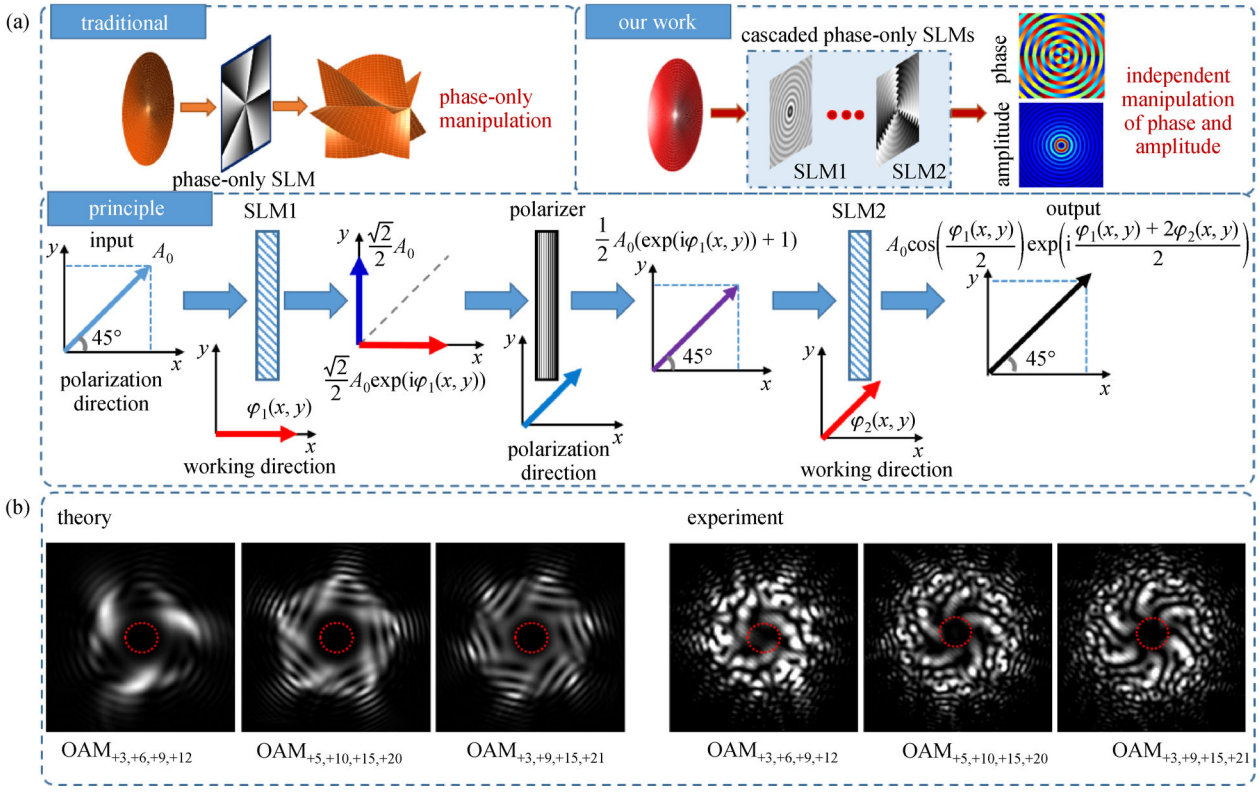

Fig. 8 (a) Concept and principle of arbitrary manipulation of spatial amplitude and phase distribution; (b) theoretical and experimental results of multiple OAM modes generation with two phase-only SLMs [37]

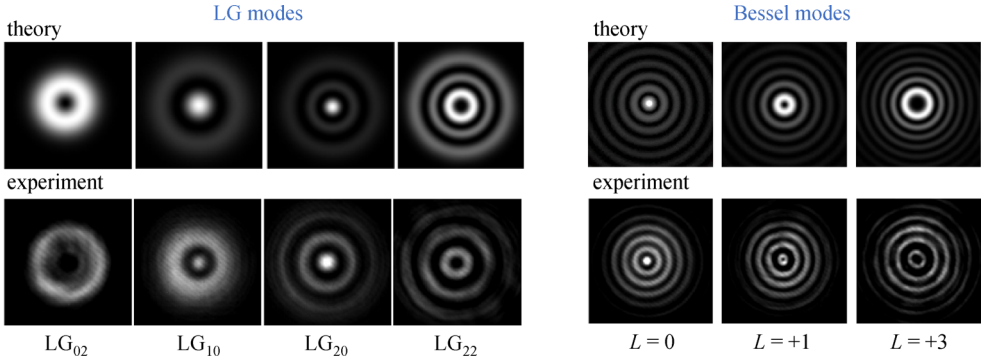

Fig. 9 Intensity profiles of the generated LG and Bessel modes by manipulating the amplitude and phase independently with two phase-only SLMs [37]

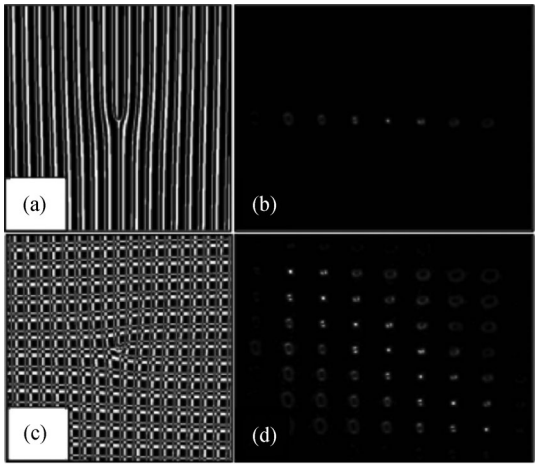

Fig. 10 (a) 1D and (c) 2D Dammann vortex gratings with (b) and (d) corresponding results [38]

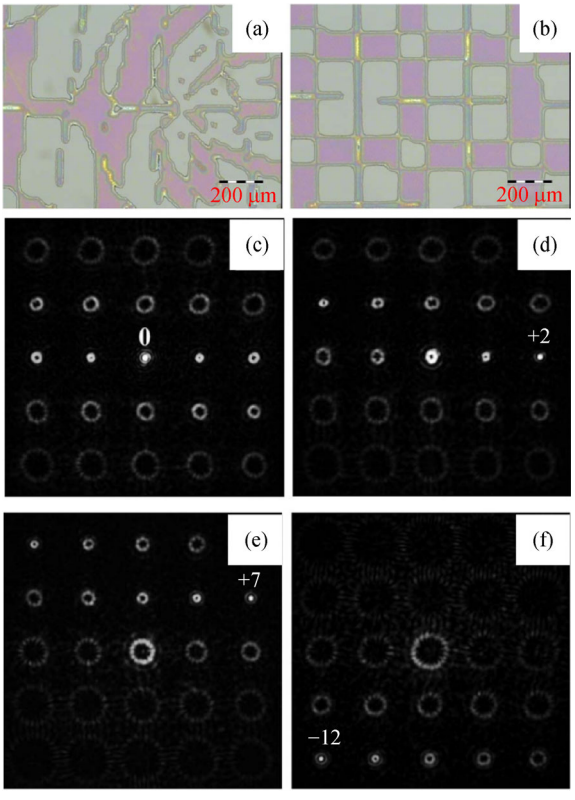

Fig. 11 (a) and (b) Center portion and typical outer areas of the fabricated Dammann vortex grating; (c)–(f) OAM detection results using the fabricated Dammann vortex grating. The topological charges of the input OAM are (c) 0, (d) − 2, (e) − 7 and (f) 12, and the labels show the detection orders [39]

waveguides with etched tilt gratings, as shown in Fig. 12. The tilt gratings facilitate flexible light emission in a wide range of directions, enabling the generation of OAM mode array above the silicon chip. The OAM mode array is also known as optical vortex (OV) lattice.

The fabricated on-chip OV lattice emitter is experimentally investigated. The experimental configuration for observing the on-chip generation of the OV lattice is illustrated in Fig. 13(a). Figure 13(b) shows the measured near-field intensity distribution of *y*-polarization light with 10° magnification coming out from the OV lattice emitter at the wavelength of 1550 nm. One can clearly see the three bright light spots emitted from the three tilt gratings. Figure 13(c) plots the measured far-field intensity distribution of *y*-polarization light with 40° magnification generated from the on-chip OV lattice emitter, which indicates the phenomenon of three-plane-wave interference and a network of dark spots. When interfering the generated OV lattice in Fig. 13(d) with another plane wave, there emerges a network of fork-like fringe patterns. One can indicate from Figs. 13(c) and 13(d) that each fork-like fringe pattern corresponds to a dark spot, verifying the successful generation of the OV lattice using the designed and fabricated compact on-chip OV lattice emitter.

2.3 *N*-to-*N* collinear OAM modes

N Gaussian modes from different angles are incident on optical element for generating *N* collinear OAM modes, which is always demanded in OAM mode multiplexing scheme. Here we introduce two methods for *N*-to-*N*

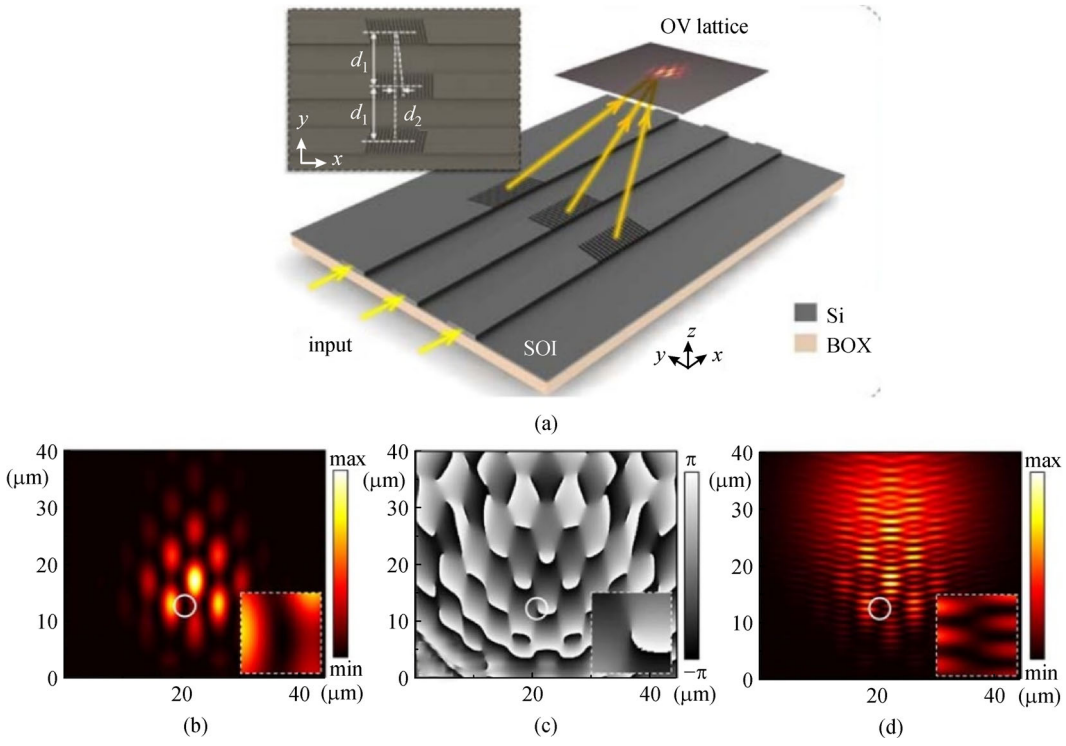

Fig. 12 (a) Concept and (b)–(d) simulation results of on-chip OAM mode array emitter on silicon platform [40]

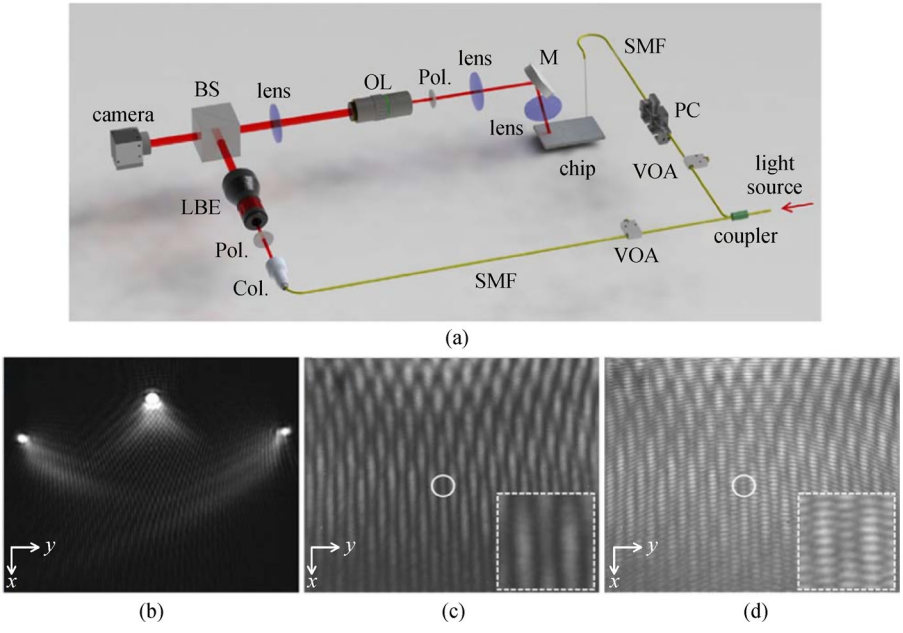

Fig. 13 (a) Experimental configuration for observing the generation of an OV lattice using the fabricated on-chip OV lattice emitter; (b) measured near-field intensity distribution of y-polarization light coming out from the emitter; (c) measured far-field intensity distribution of an OV lattice generated by the emitter. The inset shows the zoom-in intensity distribution of OVs; (d) measured intensity distribution of fork-like fringe patterns by interfering the generated OV lattice with a plane wave. The inset shows the zoom-in intensity distribution of fork-like fringe patterns [40]

collinear OAM modes.

The first one is to use Dammann vortex grating, which is the same with the previous section. Figure 14 shows a schematic of the Dammann vortex grating enabled multiple collinear OAM modes generation and multiplexing [41]. Gaussian beams with plane wavefronts are incident on the Dammann vortex grating at the angles of its diffraction orders. Therefore, along the zeroth order of diffraction, all the incident Gaussian beams are transformed into different OAM modes in the same direction. Moreover, one can also use Dammann vortex grating for OAM modes demultiplexing which is also shown in Fig. 14.

By using Dammann vortex grating, Lei et al. demonstrate independent collinear OAM channel generation, transmission and simultaneous detection [41]. 80 Tbit/s transmission capacity is achieved with uniform power distributions along all channels, with 1600 individually modulated QPSK/16-QAM data channels multiplexed by 10 OAM states, 80 wavelengths and two polarizations. The experimental results are shown in Fig. 15.

The second method is well-known as the OAM mode sorter, which is used to sort different OAM modes by two static optical elements [42–44]. The OAM mode sorter performs a log-polar to Cartesian coordinate transformation, which can convert the helically phased OAM beam into a beam with a transverse phase gradient. Then, a subsequent lens focuses each input OAM state to a different lateral position, as shown in Fig. 16 [45]. By using the OAM mode sorter, N multiplexed collinear OAM modes each with a different topological charge, can be transformed into N laterally separated and elongated spots.

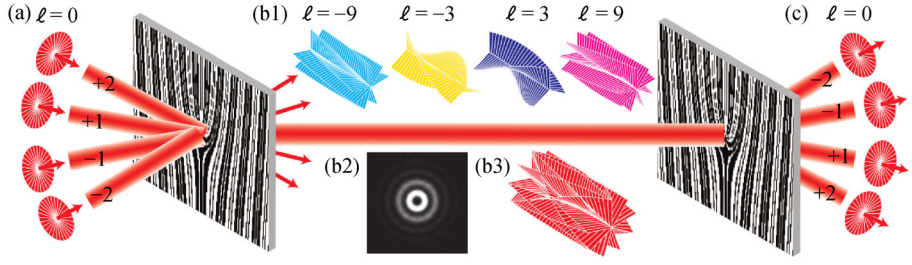

Fig. 14 Schematic of the Dammann vortex grating for multiple collinear OAM modes generation. (a) Gaussian beams incident on the grating at its diffraction angles; (b) Combined coaxial OAM beam with multiple states (b1) propagates in free space. (b2, b3) The simulated intensity pattern and wavefront of the OAM beam, respectively; (c) OAM channels are converted into Gaussian beams and are separated spatially for detection [41]

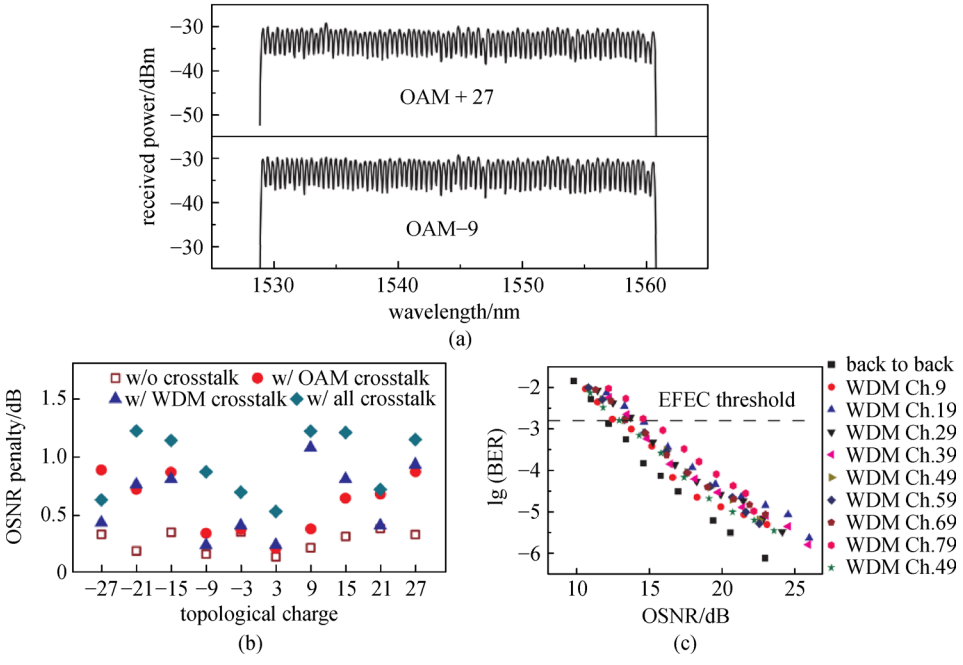

Fig. 15 Experimental results of OAM-based free-space optical communications. (a) Spectra of the OAM states + 27 and + 29 with the 80-wavelength WDM system; (b) optical signal-to-noise ratio (OSNR) penalties of the 10 OAM states; (c) bit-error rate (BER) characteristics in the same OAM channel (l = −15) for the 10 different wavelength channels [41]

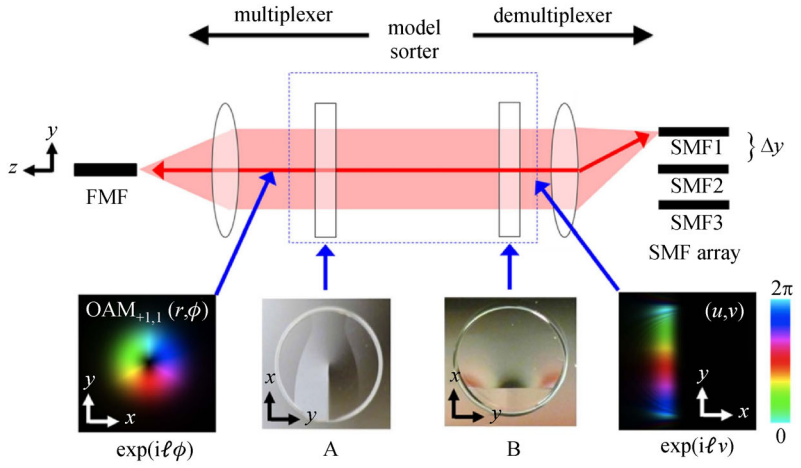

Fig. 16 Schematic of OAM mode sorter for OAM modes multiplexing and demultiplexing [45]

Importantly, when the OAM mode sorter is used in the reverse direction, N laterally separated and elongated spots can generate N collinear OAM modes, which can be used for OAM mode multiplexing. By employing OAM mode sorter, OAM modes multiplexing transmission is experimentally demonstrated. The experimental results of multiple OAM modes generation with OAM mode sorter are shown in Fig. 17.

3 Applications of multiple optical vortices

Multiple optical vortices are usually employed in optical communications. The generation of multiple OAM modes using a single element from a single input Gaussian beam is an important basic function in an OAM mode multicasting system. By using the proposed PSI algorithm, our group experimentally demonstrates 1-to-34 multicasting of an optical signal from single Gaussian mode to multiple OAM modes [46]. All 34-fold multicasted OAM channels show relatively low crosstalk (<-10 dB) from their neighboring OAM modes and achieve BER less than 2e−3. The concept and OAM mode spectrum are shown in Fig. 18.

Moreover, by designing and optimizing the complex phase pattern through the adaptive correction of feedback

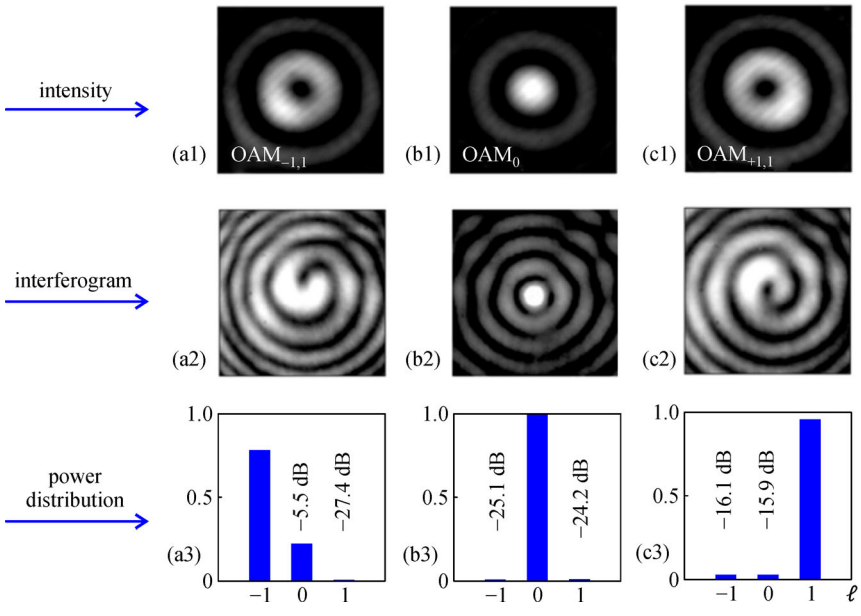

Fig. 17 Experimental results of multiple OAM modes generation with OAM mode sorter. (a1)–(c1) Intensity profiles of OAM modes generated by the OAM mode sorter; (a2)–(c2) "spiral" interferograms of each OAM mode; (a3)–(c3) OAM power spectra of each OAM mode [45]

system, the power of each multicasting OAM channel can be arbitrarily controlled. We experimentally demonstrate power-controllable multicasting from a single Gaussian mode to 6 OAM modes with different target power distributions [47]. The concept and experimental results are shown in Fig. 19.

In addition, we also demonstrate OAM mode multicasting under atmospheric turbulence condition. By employing an adaptive optics closed loop consisting of a wavefront detector and a wavefront corrector, we can successfully compensate the phase distortions [48]. The compensation can reduce power fluctuations of multicasted OAM channels and inter-channel power crosstalk, achieving a favorable communication performance. The concept and experimental results are shown in Fig. 20.

High-order Bessel beams are considered as a typical kind of light beam that can carry OAM. Remarkably, Bessel beam is widely known as a self-reconstructing light beam, which can reconstruct its electric field after passing through an obstruction. By using the proposed phase pattern designed by PSI algorithm combining with axicon phase distribution, our group reports data multicasting from a single Gaussian mode to multiple Bessel modes using a single phase-only spatial light modulator [49]. Under the obstructed path conditions, obstruction-free data-carrying *N*-fold Bessel modes multicasting is also demonstrated in the experiment. The experimental setup and results are shown in Fig. 21.

Besides optical communication applications, multiple optical vortices can also be used in non-communication areas. In 2014, Lavery et al. observed the rotational Doppler shift from a white-light source after backscattered by a spinning object [31]. They show that the magnitude of this shift is dependent upon the OAM of the light, and that

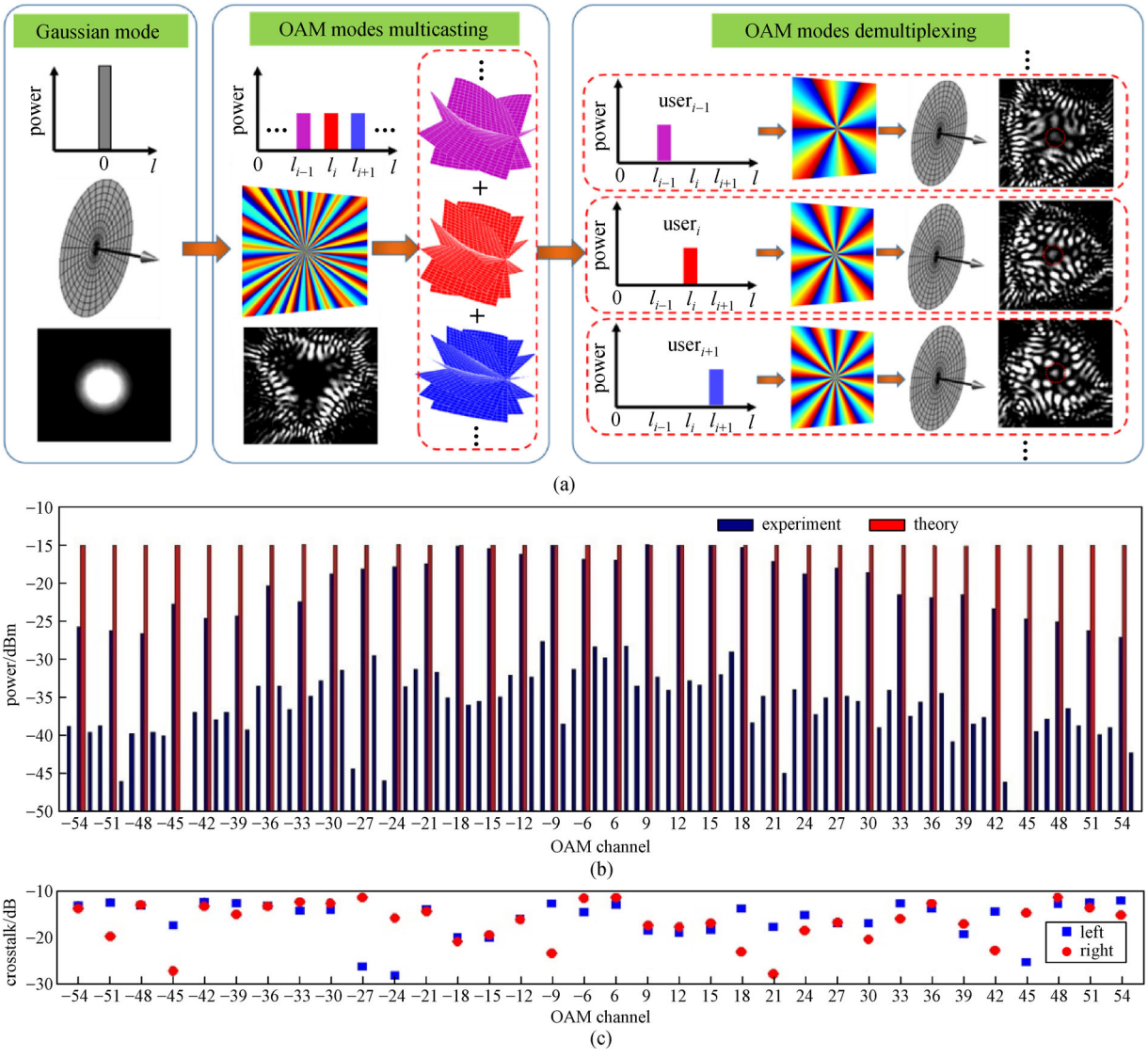

Fig. 18 Concept and experimental results of 1-to-34 OAM mode multicasting. (a) Concept and principle of 1-to-34 OAM mode multicasting; (b) measured OAM spectrum of all the multicasted OAM modes; (c) mode crosstalk of all the multicasted OAM modes [46]

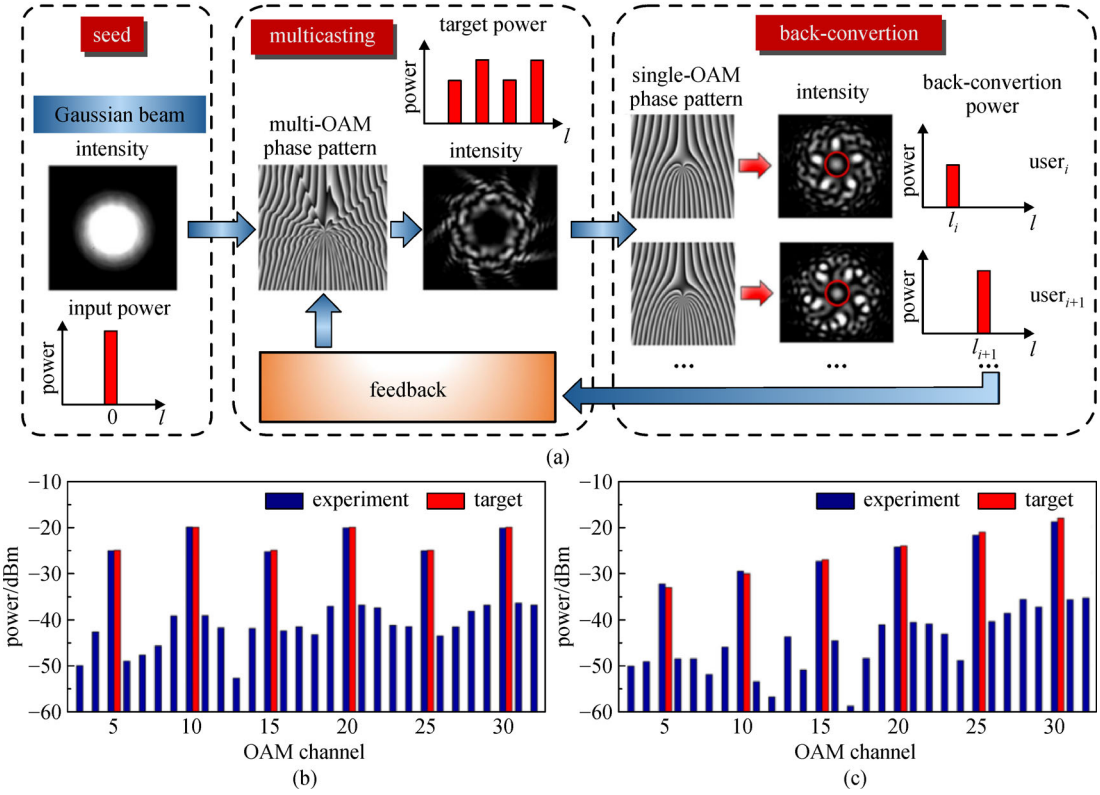

Fig. 19 (a) Concept, (b) and (c) experimental results of power-controllable OAM mode multicasting [47]

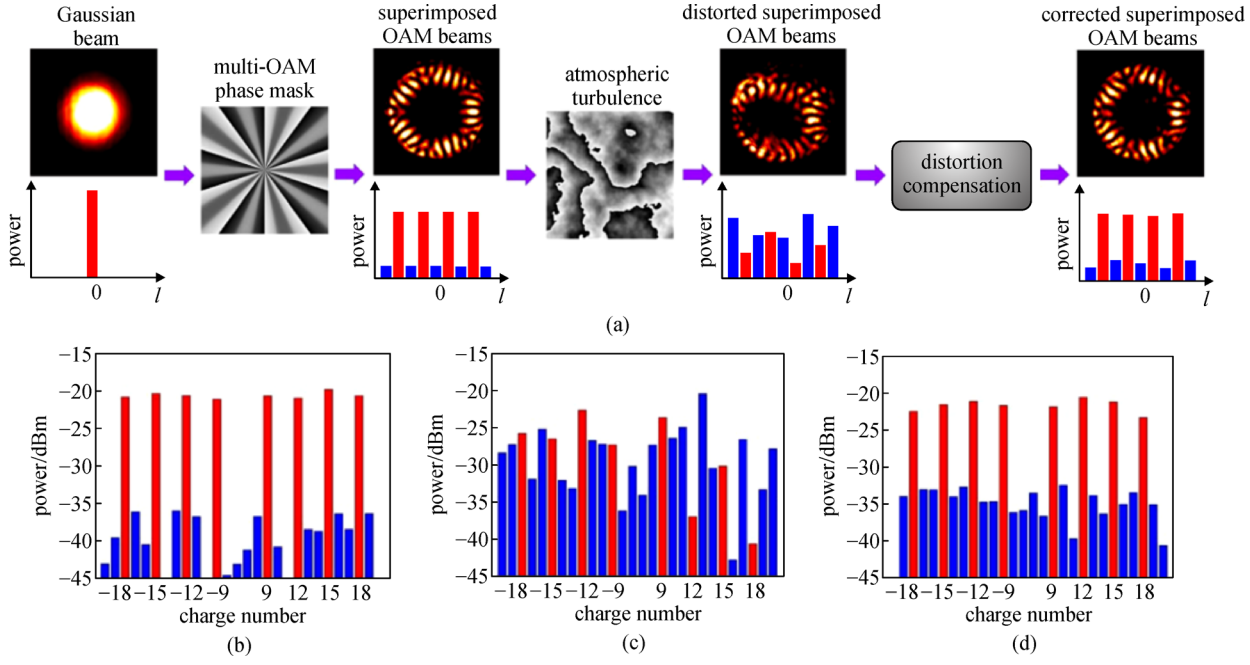

Fig. 20 (a) Concept and principle of turbulence compensation for a distorted OAM multicasting link; (b) measured OAM spectrum of all the multicasted OAM modes without turbulence; (c) measured OAM spectrum of all the multicasted OAM modes with turbulence; (d) measured OAM spectrum of all the multicasted OAM modes with turbulence-induced distortion compensation [48]

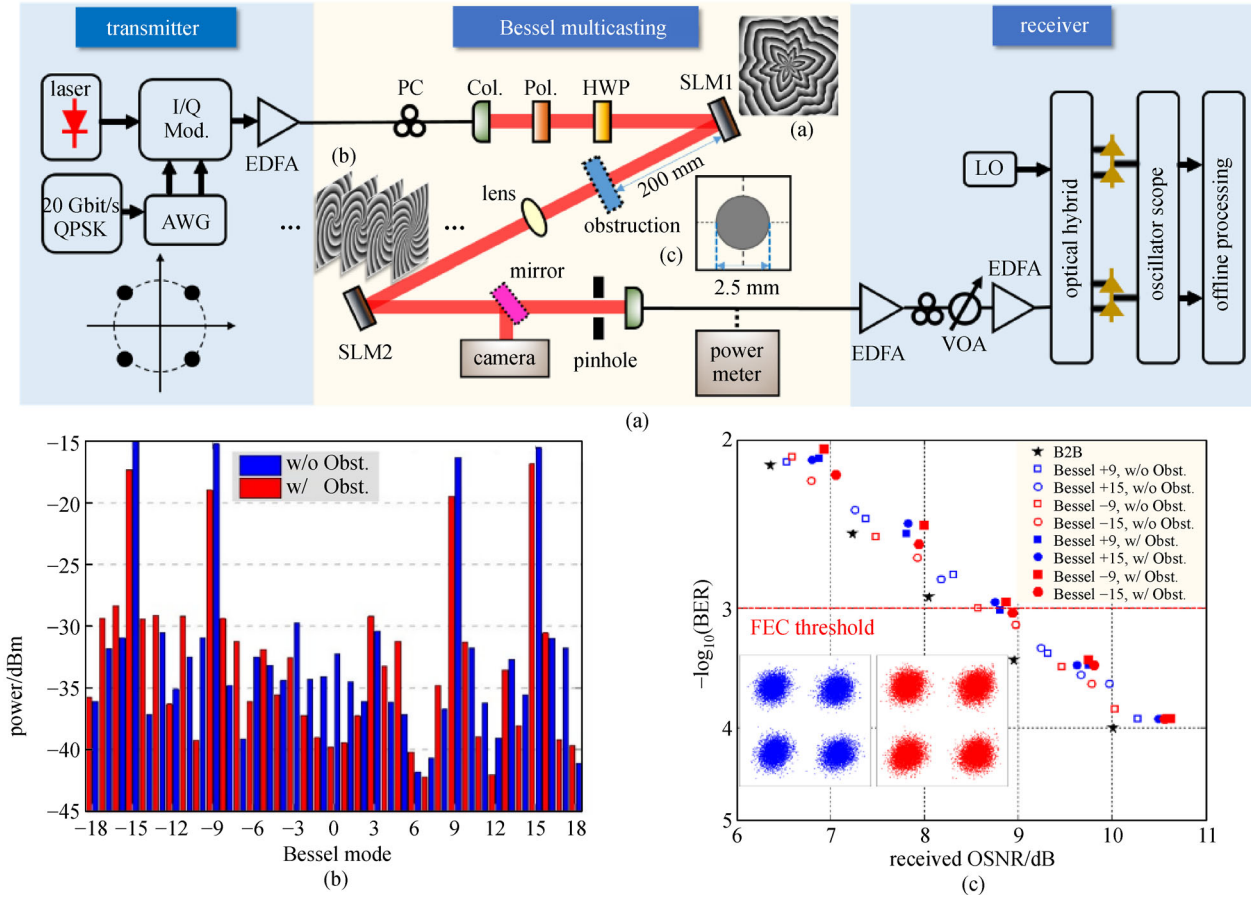

Fig. 21 (a) Experimental setup of obstruction-free data-carrying *N*-fold Bessel modes multicasting; (b) measured Bessel modes spectrum with and without obstruction; (c) measured BER performance of Bessel modes multicasting [49]

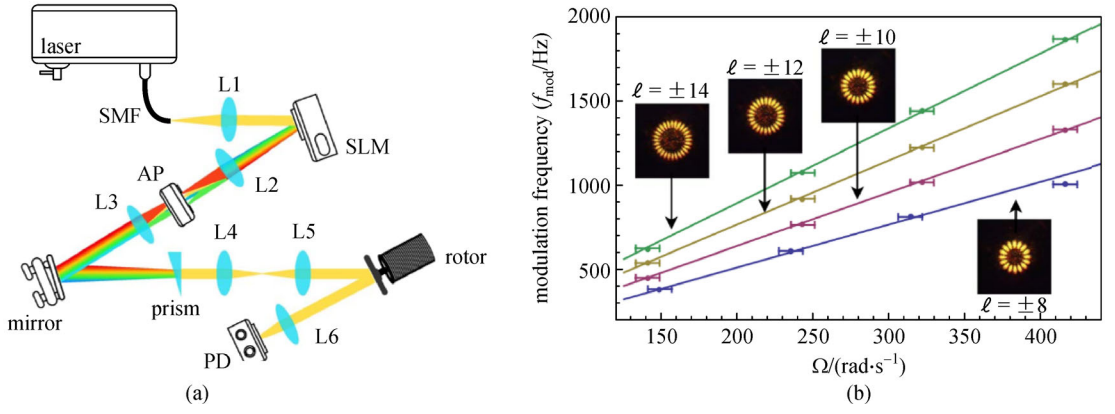

Fig. 22 (a) Experimental setup and (b) measured results of the rotational Doppler shift from a white-light source after backscattered by a spinning object. The SLM is encoded with a specific pattern to produce the superposition of different OAM states [31]

superposition of different OAM states gives rise to multiple sidebands on the shifted frequency. The observability of the frequency shift for white-light illumination highlights the potential of this rotational Doppler effect as the basis of a rotational sensor using back-scattered light. Figure 22 shows the experimental setup and measured results.

4 Trends, perspectives and challenges

In recent years, multiple optical vortices have shown great potential in optical communication systems. In this article, we review the methods of multiple optical vortices generation and its emerging applications. Different methods have been employed for multiple optical vortices

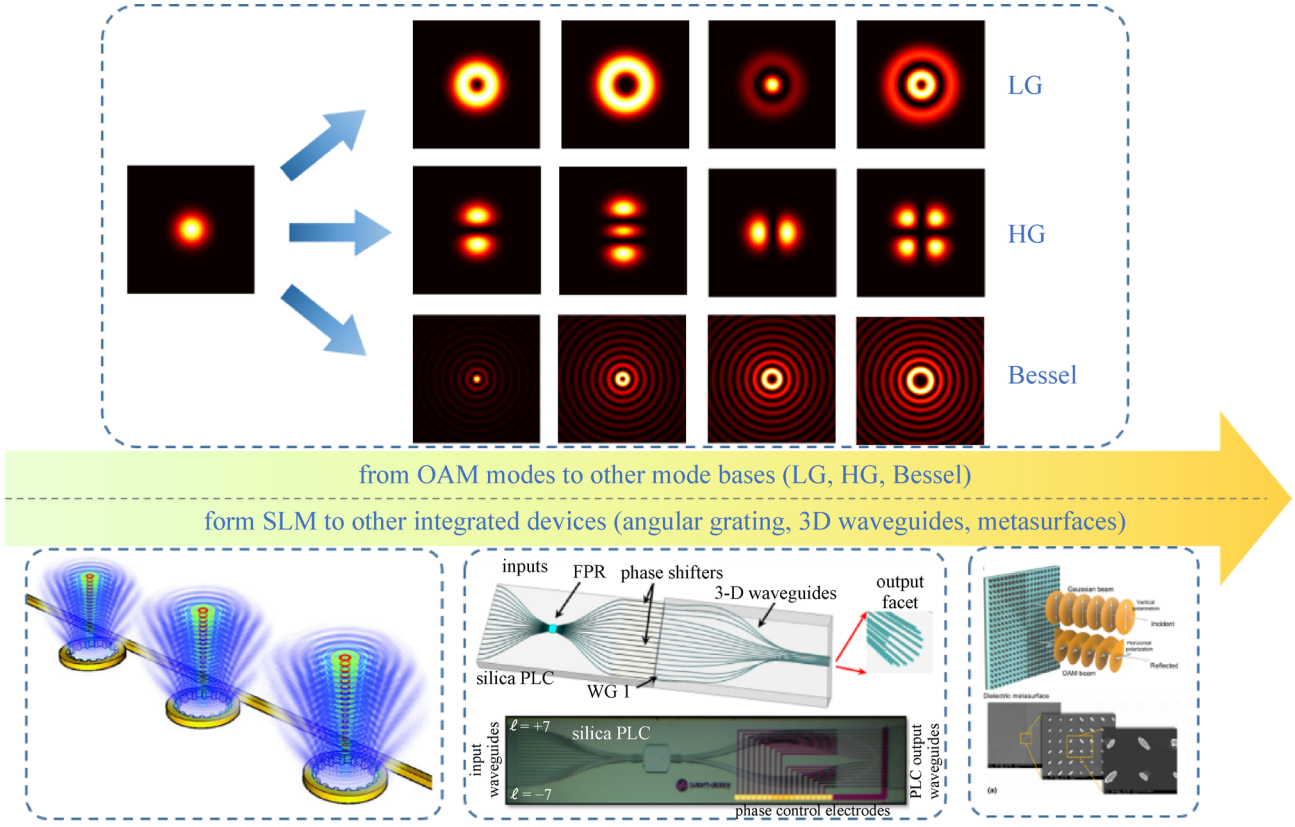

Fig. 23 Trends, perspectives and opportunities of multiple optical vortices generation [64–66]

generation, such as PSI algorithm, Dammann vortex grating, and OAM mode sorter. The experimental results show favorable performance in different applications. Figure 23 shows the trends, perspectives and opportunities of multiple optical vortices generation. In this review, we only introduce the generation of multiple OAM modes. However, other mode bases, such as LG modes, Hermite-Gaussian (HG) modes, Bessel modes and vector modes may also be desired in practical applications [50–63]. Diverse methods for the generation of multiple other mode bases are of great interest. Moreover, in the existing experiments, SLM is usually employed to control the input spatial light for generating multiple OAM modes. With future improvement, photonic integrated devices on different platforms (e.g., silicon platform) may also be designed and fabricated, which will make the system much more compact, flexible and low cost. Additionally, metamaterials and metasurfaces could also be employed to manipulate the spatial structure of light beams, which will extend the applications of multiple optical vortices and multiple other spatial modes [64–71].

Acknowledgements This work was supported by the National Natural Science Foundation of China (NSFC) (Grant Nos. 11574001, 61761130082, 11774116 and 11274131), the National Basic Research Program of China (973 Program) (No. 2014CB340004), the Royal Society-Newton Advanced Fellowship, the National Program for Support of Top-notch Young Professionals, the Yangtze River Excellent Young Scholars Program, the Natural Science Foundation of Hubei Province of China (No. 2018CFA048), and the Program for HUST Academic Frontier Youth Team (No. 2016QYTD05).

References

1. Allen L, Beijersbergen M W, Spreeuw R J C, Woerdman J P. Orbital angular momentum of light and the transformation of Laguerre-Gaussian laser modes. Physical Review A, 1992, 45(11): 8185–8189
2. Yao A M, Padgett M J. Orbital angular momentum: origins, behavior and applications. Advances in Optics and Photonics, 2011, 3(2): 161–204
3. Franke-Arnold S, Allen L, Padgett M. Advances in optical angular momentum. Laser & Photonics Reviews, 2008, 2(4): 299–313
4. Dholakia K, Čižmár T. Shaping the future of manipulation. Nature Photonics, 2011, 5(6): 335–342
5. Paterson L, MacDonald M P, Arlt J, Sibbett W, Bryant P E, Dholakia K. Controlled rotation of optically trapped microscopic particles. Science, 2001, 292(5518): 912–914
6. Padgett M, Bowman R. Tweezers with a twist. Nature Photonics, 2011, 5(6): 343–348
7. Dennis M R, King R P, Jack B, O'Holleran K, Padgett M J. Isolated optical vortex knots. Nature Physics, 2010, 6(2): 118–121
8. Bernet S, Jesacher A, Fürhapter S, Maurer C, Ritsch-Marte M.

Quantitative imaging of complex samples by spiral phase contrast microscopy. Optics Express, 2006, 14(9): 3792–3805
9. Mair A, Vaziri A, Weihs G, Zeilinger A. Entanglement of the orbital angular momentum states of photons. Nature, 2001, 412(6844): 313–316
10. Gibson G, Courtial J, Padgett M, Vasnetsov M, Pas'ko V, Barnett S, Franke-Arnold S. Free-space information transfer using light beams carrying orbital angular momentum. Optics Express, 2004, 12(22): 5448–5456
11. Wang J, Yang J Y, Fazal I M, Ahmed N, Yan Y, Huang H, Ren Y, Yue Y, Dolinar S, Tur M, Willner A E. Terabit free-space data transmission employing orbital angular momentum multiplexing. Nature Photonics, 2012, 6(7): 488–496
12. Bozinovic N, Yue Y, Ren Y, Tur M, Kristensen P, Huang H, Willner A E, Ramachandran S. Terabit-scale orbital angular momentum mode division multiplexing in fibers. Science, 2013, 340(6140): 1545–1548
13. Willner A E, Wang J, Huang H. A different angle on light communications. Science, 2012, 337(6095): 655–656
14. Krenn M, Handsteiner J, Fink M, Fickler R, Ursin R, Malik M, Zeilinger A. Twisted light transmission over 143 km. Proceedings of the National Academy of Sciences of the United States of America, 2016, 113(48): 13648–13653
15. Wang A, Zhu L, Chen S, Du C, Mo Q, Wang J. Characterization of LDPC-coded orbital angular momentum modes transmission and multiplexing over a 50-km fiber. Optics Express, 2016, 24(11): 11716–11726
16. Willner A E, Huang H, Yan Y, Ren Y, Ahmed N, Xie G, Bao C, Li L, Cao Y, Zhao Z, Wang J, Lavery M P J, Tur M, Ramachandran S, Molisch A F, Ashrafi N, Ashrafi S. Optical communications using orbital angular momentum beams. Advances in Optics and Photonics, 2015, 7(1): 66–106
17. Wang J. Advances in communications using optical vortices. Photonics Research, 2016, 4(5): B14–B28
18. Wang J. Data information transfer using complex optical fields: a review and perspective. Chinese Optics Letters, 2017, 15(3): 030005–030009
19. Zhu L, Liu J, Mo Q, Du C, Wang J. Encoding/decoding using superpositions of spatial modes for image transfer in km-scale few-mode fiber. Optics Express, 2016, 24(15): 16934–16944
20. Zhu L, Wang A, Chen S, Liu J, Mo Q, Du C, Wang J. Orbital angular momentum mode groups multiplexing transmission over 2.6-km conventional multi-mode fiber. Optics Express, 2017, 25(21): 25637–25645
21. Wang A, Zhu L, Wang L, Ai J, Chen S, Wang J. Directly using 8.8-km conventional multi-mode fiber for 6-mode orbital angular momentum multiplexing transmission. Optics Express, 2018, 26(8): 10038–10047
22. Wang A, Zhu L, Liu J, Du C, Mo Q, Wang J. Demonstration of hybrid orbital angular momentum multiplexing and time-division multiplexing passive optical network. Optics Express, 2015, 23(23): 29457–29466
23. Jung Y, Kang Q, Zhou H, Zhang R, Chen S, Wang H, Yang Y, Jin X, Payne F P, Alam S, Richardson D J. Low-loss 25.3 km few-mode ring-core fiber for mode-division multiplexed transmission. Journal of Lightwave Technology, 2017, 35(8): 1363–1368
24. Zhu G, Hu Z, Wu X, Du C, Luo W, Chen Y, Cai X, Liu J, Zhu J, Yu S. Scalable mode division multiplexed transmission over a 10-km ring-core fiber using high-order orbital angular momentum modes. Optics Express, 2018, 26(2): 594–604
25. Zhu L, Zhu G, Wang A, Wang L, Ai J, Chen S, Du C, Liu J, Yu S, Wang J. 18 km low-crosstalk OAM + WDM transmission with 224 individual channels enabled by a ring-core fiber with large high-order mode group separation. Optics Letters, 2018, 43(8): 1890–1893
26. Padgett M, Courtial J, Allen L. Light's orbital angular momentum. Physics Today, 2004, 57(5): 35–40
27. Su T, Scott R P, Djordjevic S S, Fontaine N K, Geisler D J, Cai X, Yoo S J B. Demonstration of free space coherent optical communication using integrated silicon photonic orbital angular momentum devices. Optics Express, 2012, 20(9): 9396–9402
28. Wang A, Zhu L, Wang L, Ai J, Chen S, Wang J. Directly using 8.8-km conventional multi-mode fiber for 6-mode orbital angular momentum multiplexing transmission. Optics Express, 2018, 26(8): 10038–10047
29. Zhu L, Wang A, Chen S, Liu J, Mo Q, Du C, Wang J. Orbital angular momentum mode groups multiplexing transmission over 2.6-km conventional multi-mode fiber. Optics Express, 2017, 25(21): 25637–25645
30. Lavery M P, Speirits F C, Barnett S M, Padgett M J. Detection of a spinning object using light's orbital angular momentum. Science, 2013, 341(6145): 537–540
31. Lavery M, Barnett S, Speirits F, Padgett M. Observation of the rotational doppler shift of a white-light, orbital-angular-momentum-carrying beam backscattered from a rotating body. Optica, 2014, 1 (1): 1–4
32. Belmonte A, Rosales-Guzmán C, Torres J P. Measurement of flow vorticity with helical beams of light. Optica, 2015, 2(11): 1002–1005
33. Fang L, Padgett M J, Wang J. Sharing a common origin between the rotational and linear Doppler effects. Laser & Photonics Reviews, 2017, 11(6): 1700183
34. Yan Y, Yue Y, Huang H, Ren Y, Ahmed N, Tur M, Dolinar S, Willner A. Multicasting in a spatial division multiplexing system based on optical orbital angular momentum. Optics Letters, 2013, 38(19): 3930–3933
35. Lin J, Yuan X C, Tao S H, Burge R E. Collinear superposition of multiple helical beams generated by a single azimuthally modulated phase-only element. Optics Letters, 2005, 30(24): 3266–3268
36. Zhu L, Wang J. Simultaneous generation of multiple orbital angular momentum (OAM) modes using a single phase-only element. Optics Express, 2015, 23(20): 26221–26233
37. Zhu L, Wang J. Arbitrary manipulation of spatial amplitude and phase using phase-only spatial light modulators. Scientific Reports, 2014, 4(1): 7441
38. Moreno I, Davis J A, Cottrell D M, Zhang N, Yuan X C. Encoding generalized phase functions on Dammann gratings. Optics Letters, 2010, 35(10): 1536–1538
39. Zhang N, Yuan X C, Burge R E. Extending the detection range of optical vortices by Dammann vortex gratings. Optics Letters, 2010, 35(20): 3495–3497
40. Du J, Wang J. Design of on-chip N-fold orbital angular momentum

multicasting using V-shaped antenna array. Scientific Reports, 2015, 5(1): 9662
41. Lei T, Zhang M, Li Y, Jia P, Liu G N, Xu X, Li Z, Min C, Lin J, Yu C, Niu H, Yuan X C. Massive individual orbital angular momentum channels for multiplexing enabled by Dammann gratings. Light, Science & Applications, 2015, 4(3): e257
42. Berkhout G C G, Lavery M P J, Courtial J, Beijersbergen M W, Padgett M J. Efficient sorting of orbital angular momentum states of light. Physical Review Letters, 2010, 105(15): 153601
43. Mirhosseini M, Malik M, Shi Z, Boyd R W. Efficient separation of the orbital angular momentum eigenstates of light. Nature Communications, 2013, 4(1): 2781
44. Lavery M P J, Berkhout G C G, Courtial J, Padgett M J. Measurement of the light orbital angular momentum spectrum using an optical geometric transformation. Journal of Optics, 2011, 13(6): 064006
45. Huang H, Milione G, Lavery M P, Xie G, Ren Y, Cao Y, Ahmed N, An Nguyen T, Nolan D A, Li M J, Tur M, Alfano R R, Willner A E. Mode division multiplexing using an orbital angular momentum mode sorter and MIMO-DSP over a graded-index few-mode optical fibre. Scientific Reports, 2015, 5: 14931
46. Li S, Wang J, Zhang X, Zhu L, Li C, Yang Q. Demonstration of simultaneous 1-to-34 multicasting of OFDM/OQAM 64-QAM signal from single Gaussian mode to multiple orbital angular momentum (OAM) modes. In: Proceedings of Asia Communications and Photonics Conference 2013 Postdeadline. Optical Society of America, 2013, paper AF2E.5
47. Li S, Wang J. Adaptive power-controllable orbital angular momentum (OAM) multicasting. Scientific Reports, 2015, 5(1): 9677
48. Li S, Wang J. Compensation of a distorted N-fold orbital angular momentum multicasting link using adaptive optics. Optics Letters, 2016, 41(7): 1482–1485
49. Zhu L, Wang J. Demonstration of obstruction-free data-carrying N-fold Bessel modes multicasting from a single Gaussian mode. Optics Letters, 2015, 40(23): 5463–5466
50. Durnin J, Miceli J Jr, Eberly J H. Diffraction-free beams. Physical Review Letters, 1987, 58(15): 1499–1501
51. McGloin D, Dholakia K. Bessel beams: diffraction in a new light. Contemporary Physics, 2005, 46(1): 15–28
52. Durnin J, Miceli J J Jr, Eberly J H. Comparison of Bessel and Gaussian beams. Optics Letters, 1988, 13(2): 79
53. Du J, Wang J. High-dimensional structured light coding/decoding for free-space optical communications free of obstructions. Optics Letters, 2015, 40(21): 4827–4830
54. Zhu L, Wang J. Demonstration of obstruction-free data-carrying N-fold Bessel modes multicasting from a single Gaussian mode. Optics Letters, 2015, 40(23): 5463–5466
55. Chen S, Li S, Zhao Y, Liu J, Zhu L, Wang A, Du J, Shen L, Wang J. Demonstration of 20-Gbit/s high-speed Bessel beam encoding/decoding link with adaptive turbulence compensation. Optics Letters, 2016, 41(20): 4680–4683
56. Li S, Wang J. Adaptive free-space optical communications through turbulence using self-healing Bessel beams. Scientific Reports, 2017, 7(1): 43233
57. Zhan Q. Cylindrical vector beams from mathematical concepts to applications. Advances in Optics and Photonics, 2009, 1(1): 1–57
58. Milione G, Lavery M P J, Huang H, Ren Y, Xie G, Nguyen T A, Karimi E, Marrucci L, Nolan D A, Alfano R R, Willner A E. 4 × 20 Gbit/s mode division multiplexing over free space using vector modes and a q-plate mode (de)multiplexer. Optics Letters, 2015, 40 (9): 1980–1983
59. Zhao Y, Wang J. High-base vector beam encoding/decoding for visible-light communications. Optics Letters, 2015, 40(21): 4843–4846
60. Liu J, Li S, Zhu L, Wang A, Chen S, Klitis C, Du C, Mo Q, Sorel M, Yu S, Cai X, Wang J. Direct fiber vector eigenmode multiplexing transmission seeded by integrated optical vortex emitters. Light, Science & Applications, 2018, 7(3): 17148
61. Shwartz S, Golub M, Ruschin S. Diffractive optical elements for mode-division multiplexing of temporal signals with the aid of Laguerre-Gaussian modes. Applied Optics, 2013, 52(12): 2659–2669
62. Xie G, Ren Y, Yan Y, Huang H, Ahmed N, Li L, Zhao Z, Bao C, Tur M, Ashrafi S, Willner A E. Experimental demonstration of a 200-Gbit/s free-space optical link by multiplexing Laguerre-Gaussian beams with different radial indices. Optics Letters, 2016, 41(15): 3447–3450
63. O'Neil A T, Courtial J. Mode transformations in terms of the constituent Hermite-Gaussian or Laguerre-Gaussian modes and the variable-phase mode converter. Optics Communications, 2000, 181 (1–3): 35–45
64. Cai X, Wang J, Strain M J, Johnson-Morris B, Zhu J, Sorel M, O'Brien J L, Thompson M G, Yu S. Integrated compact optical vortex beam emitters. Science, 2012, 338(6105): 363–366
65. Guan B, Scott R P, Qin C, Fontaine N K, Su T, Ferrari C, Cappuzzo M, Klemens F, Keller B, Earnshaw M, Yoo S J B. Free-space coherent optical communication with orbital angular, momentum multiplexing/demultiplexing using a hybrid 3D photonic integrated circuit. Optics Express, 2014, 22(1): 145–156
66. Du J, Wang J. Dielectric metasurfaces enabling twisted light generation/detection/(de)multiplexing for data information transfer. Optics Express, 2018, 26(10): 13183–13194
67. Zhao Z, Wang J, Li S, Willner A E. Metamaterials-based broadband generation of orbital angular momentum carrying vector beams. Optics Letters, 2013, 38(6): 932–934
68. Yang Y, Wang W, Moitra P, Kravchenko I I, Briggs D P, Valentine J. Dielectric meta-reflectarray for broadband linear polarization conversion and optical vortex generation. Nano Letters, 2014, 14(3): 1394–1399
69. Karimi E, Schulz S A, De Leon I, Qassim V, Upham J, Boyd R W. Generating optical orbital angular momentum at visible wavelengths using a plasmonic metasurface. Light, Science & Applications, 2014, 3(5): e167
70. Wang J. Metasurfaces enabling structured light manipulation: advances and perspectives. Chinese Optics Letters, 2018, 16(5): 050006
71. Li G, Kang M, Chen S, Zhang S, Pun E Y, Cheah K W, Li J. Spin-enabled plasmonic metasurfaces for manipulating orbital angular momentum of light. Nano Letters, 2013, 13(9): 4148–4151

Jian Wang received the Ph.D. degree in physical electronics from the Wuhan National Laboratory for Optoelectronics, Huazhong University of Science and Technology, Wuhan, China, in 2008. He worked as a Postdoctoral Research Associate in the optical communications laboratory in the Ming Hsieh Department of Electrical Engineering of the Viterbi School of Engineering, University of Southern California, Los Angeles, California, USA, from 2009 to 2011. He is currently a professor at the Wuhan National Laboratory for Optoelectronics, Huazhong University of Science and Technology, Wuhan, China. Jian Wang has received the following representative honors/awards: Royal Society-Newton Advanced Fellowship, Yangtze River Excellent Young Scholars, National Program for Support of Top-notch Young Professionals, National Science Foundation for Excellent Young Scholars, New Century Excellent Talents in University of Ministry of Education of China, and the First Prize in Natural Science Award of Ministry of Education of China.

Jian Wang has devoted his research efforts to innovations in photonic integrated devices and frontiers of high-speed optical communications and optical signal processing. He has more than 300 publications in total, including 7 book chapters, 5 special issues, 7 review articles, 10 invited papers, 80 tutorial/keynote/invited talks (invited talk at OFC2014, tutorial talk at OFC2016), 12 postdeadline papers, and more than 100 journal papers published on *Science*, *Nature Photonics*, *Science Advances*, *Light: Science & Applications*, *Laser & Photonics Reviews*, *Optica*, *Scientific Reports*, *Optics Express*, *Optics Letters*, *Photonics Research*, etc. Jian Wang serves as the Topical Editor of *Optics Letters*, Topic Editor of *Chinese Optics Letters*, and Area Editor of *Microwave and Optical Technology Letters*. Jian Wang is also the frequent reviewer for more than 30 journals such as *Nature Photonics*, *Nature Communications*, *Advanced Materials*, *Light: Science & Applications*, *Physical Review Letters*, *Laser & Photonics Reviews*, *Optica*, *ACS Photonics*, *Advanced Optical Materials*, *Optics Express*, *Optics Letters*, *Scientific Reports*, etc.